sPREDICTION OF THROMBUS FORMATION USING VORTICAL STRUCTURES PRESENTATION IN STANFORD TYPE B AORTIC DISSECTION: A PRELIMINARY STUDY USING CFD APPROACH

Wan Naimah Wan Ab Naim[1,*], Poo Balan Ganesan[2], Zhonghua Sun[3], Yih Miin Liew[1], Yi Qian[4], Chang-Joon Lee[4], Shirley Jansen[5], Shahrul Amry Hashim[6], Einly Lim[1]

1 Department of Biomedical Engineering, Faculty of Engineering Building, University of Malaya, 50603 Kuala Lumpur, Malaysia.

2 Department of Mechanical Engineering, Faculty of Engineering Building, University of Malaya, 50603 Kuala Lumpur, Malaysia.

3 Department of Medical Radiation Sciences, Curtin University, Perth, 6845 Australia.

4 The Australian School of Advanced Medicine,2 Technology Place, Macquarie University NSW 2109, Australia.

5 Department of Vascular Surgery**,** Sir Charles Gairdner Hospital Nedlands, 6009**,** Australia.

6 Department of Surgery, Faculty of Medicine Building, University of Malaya, 50603 Kuala Lumpur, Malaysia

*Author for correspondence (naimah88@siswa.um.edu.my)

ABSTRACT

False lumen patency has been recognized as the key determinant of aneurismal dilatation and rupture, whereas complete thrombosis has been proven clinically to improve disease outcomes. However, to date, there is no definitive method that could predict false lumen thrombosis in Stanford type B aortic dissection patient. The present study aims to use the evolution of vortical structures throughout a cardiac cycle and its interaction with the wall shear stress (WSS) to illustrate the potential mechanism behind the formation of thrombus and predict its highly possible location in an aortic dissection patient. A three-dimensional (3D) patient-specific Stanford Type B aortic dissection domain was generated from computed tomography (CT) angiographic images. The effects of false lumen size on vortical structures and the subsequent risk of thrombus formation were investigated. The Carreau-Yasuda model, representing non-Newtonian fluid property was used to study the difference between Newtonian and non-Newtonian fluid settings on vortical structures. Based on our analysis, we predicted that the formation and thickening of thrombus is very much likely to occur at the posterior false lumen wall, distal to the entry tear region, in the patient. Higher λ_2 intensity, associated with a higher maximum WSS and a lower minimum WSS, was achieved with an increase in the false lumen size, and we believed that this increases the risk of thrombus formation and thus aneurismal dilatation. On the other hand, percentage of flow entering the false lumen increased with an increase in the false lumen size, leading to a downward shift of the areas of thrombus formation along the false lumen wall.

1.0   INTRODUCTION

Aortic dissection, characterized by separation of the aortic wall layers into true and false lumens, may lead to serious complications including aortic rupture, myocardial ischemia, hypotension/shock, end organ ischemia and death [1]. Aortic dissection can be classified into Stanford type A dissection which involves the ascending aorta and Stanford type B dissection which involves the descending aorta [2]. Generally, patients without complications are treated medically with hypotensive drugs during the acute phase. However, it has been reported that 25% of these patients develop subsequent aneurismal dilatation or rupture during the chronic phase, thus requiring surgical intervention [3]. Accurate prediction of possible acute complications and degenerative aneurysm in patients with Type B dissection allows early placement of stent graft to facilitate aortic stabilization and remodeling in these subgroup of patients [4]. Although a number of variables identifiable on the computed tomography scan, including large primary intimal tear, false lumen diameter, and patency of false lumen, have been suggested to be risk factors for rapid aneurismal growth in aortic dissection patients [4, 5], early prediction of late complications in aortic dissection remains challenging.

False lumen patency has been recognized as a primary predictor of aneurismal dilatation [4] while complete thrombosis was proven clinically to improve disease outcomes [3]. Meanwhile, recent studies have reported an increase in the risk of death (by a factor of 2.7) in aortic dissection patients with partial thrombosis in the false lumen [6, 7]. Intraluminal thrombosis was associated with hypoxia of the arterial wall, which leads to increased local inflammation, neurovascularization and localized wall weakening [7, 8], and thus its subsequent rupture [8]. Despite evidences showing a close correlation between false lumen thrombosis and the progression of false lumen aneurysm [6], mechanisms behind false lumen thrombosis remains unclear and there is no definitive method in predicting spontaneous false lumen thrombosis [4].

To date, limited simulation studies have attempted to relate slow and recirculating flow [9-11] as well as long particle residence time [4] with false lumen thrombosis in uncomplicated aortic dissection patients. However, the assumption that thrombus would form in regions with low velocity or negligible fluid motion is contradicted by Biasetti, Hussain and Gasser [12], who reported that despite

having low flow velocities and WSS, intra-luminal thrombus (ILT) is seldom observed in the aneurysmatic bulge of the saccular abdominal aortic aneurysm (AAA) cases. To the contrary, Biasetti *et al.* [12] applied the particle laden flow theory to prove the importance of vortical structures (VSs) in analyzing platelet motion and explaining the formation of ILT [13] in patients with AAA. A series of numerical as well as experimental studies using digital particle image velocimetry on stenosed carotid artery have also been performed by another group [14-16], which quantitatively depicted the process by which fluid dynamic mechanisms (involving vortices and shear stress) led to platelet activation, aggregation and deposition, and the subsequent formation of thrombin. In these studies, the platelet activity state assay was used to measure flow-induced platelet activation. Compared to AAA and carotid artery, the shape of the dissected aorta is much more complex, with the presence of false lumen which initiated from the entry tear, extended proximally to the arch, forming a coarctation proximal to the tear, and spiraled distally around the true lumen [3]. This complicated geometrical feature resulted in complex flow phenomenon, including substantive recirculating and disturbed flow, especially in the false lumen region [3].

In a study performed on fifty-five consecutive patients with acute type B aortic dissection, Chang *et al.* reported that maximal false lumen area and branch-vessel involvement were independent predictors of in-hospital complications [17]. In relation to this, Trimarchi *et al.* revealed that aortic dissection patients with larger initial aortic diameter have an increased chance of thrombosis in the false lumen region [6]. Although several simulation studies have been performed to investigate the variations in hemodynamics brought about by false lumen dilatation [1, 9], conflicting results have been obtained. Using computational fluid dynamics (CFD) study, Karmonik *et al.* [9] demonstrated a significant reduction in the average total pressure and WSS at the thoracic posterior false lumen wall due to false lumen aneurismal dilatation during follow up. Contradictory findings were observed by Tse *et al.* [1], who reported higher pressure in the false lumen region in the post-aneurismal aorta as compared to the pre-aneurismal aorta, and they attributed this to false luminal dilation and a reduction in the velocity value. The differences in these simulation results may be explained by the fact that geometries obtained through a longitudinal study (at initial examination and follow up scans) may not

only involve a change in the false lumen diameter, but also variations in the tear configurations which were reported to affect overall hemodynamics [4].

In the present study, we attempted to carry out a preliminary investigation which uses vortical structures as a potential parameter to describe the mechanism behind the formation of thrombus and to predict its location in aortic dissection patients, using patient-specific geometry of a Type B aortic dissection patient. Detailed distributions of vortical structures as well as WSS in the false lumen region were analyzed throughout a cardiac cycle, both qualitatively and quantitatively. In order to investigate the effect of false lumen size on the hemodynamic variables and the subsequent effect to thrombosis, the original geometry was modified by varying the diameter of the false lumen region. Furthermore, the Carreau-Yasuda model, representing non-Newtonian fluid property was used to study the difference between Newtonian and non-Newtonian fluid settings on vortical structures.

2.0   METHODOLOGY

2.1   Model Geometry

CT images of a Stanford Type B aortic dissection patient, with false lumen ended at the descending aorta region, were manually segmented to generate a 3D model (i.e. Geometry 1), as shown in Figure 1 and Table 1. This study was approved by the Curtin University Human Research Ethics Committee. Diameters of the descending aorta (including both true and false lumens) at planes A, B, and C, as illustrated in Figure 1 and Table 1, were 37.9, 56.0 and 41.8 mm, respectively. On the other hand, diameters of the false lumen at planes A, B, and C were 25.2, 24.8 and 26.0 respectively. To investigate the effect of false lumen size on the hemodynamic variables, the original geometry was modified by increasing (Geometry 2) and decreasing (Geometry 3) the diameter of the false lumen region. Specifically, the false lumen in Geometry 1 was initially separated from the true lumen using the Boolean subtraction operation. The false lumen region opposite to the line of intimal flap was then enlarged or shrunk through morphological dilation or erosion by 1-3 pixels to generate Geometry 2 and 3 as shown in Figure 1. Due to irregular shapes and orientation of the geometry, a variation of 5% to 15% changes in size was estimated along the false lumen. An increase in the total aortic diameter, of up to 4 mm or approximately 12%, is likely to happen during the follow up periods for patients with Type B aortic dissection [18]. Diameters of the cross-sections at Plane A, Plane B and Plane C were measured at perpendicular distance to the line of the intimal flap. The respective sizes of the false lumen as well as the descending aorta at the three different planes for the original and modified geometries are listed in Table 1. The height and width of the entry tear were 18.4 and 44.6 mm respectively.

2.2   Model Settings

The aortic wall was assumed to be rigid, based on in vivo data obtained from 32 type B aortic dissection patients which showed a significant reduction (12%) in the vessel wall distensibility [19]. No-slip boundary condition was applied at the aortic wall, whereby the fluid near the wall boundary has zero velocity relative to the boundary. Two different fluid properties, i.e. Newtonian and Carreau-Yasuda (representing non-Newtonian) models were used in the present study. The Carreau-Yasuda

model was chosen, as previous experimental studies [20] have shown that its shear thinning properties match that of the blood, and it is able to predict velocity distribution in the carotid bifurcation accurately. For the Newtonian model, blood was assumed to be homogenous and incompressible with a dynamic viscosity of 0.00371 Pa.s and a density of 1060 kg/m^3 [1]. The Carreau-Yasuda model [12, 20], on the other hand, is defined as:

$$\frac{\mu-\mu_\infty}{\mu_0-\mu_\infty} = [1 + (\lambda\gamma)^a]^{(n-1)/a} \tag{1}$$

where $\gamma = \sqrt{2D}$ with D denoting the scalar shear rate, μ_0 is the zero shear rate limit (0.16 Pa.s), μ_∞ is the infinite shear rate limit (0.0035 Pa.s), λ is the relaxation time (8.2 s), n is the power index (0.2128) and a is the width of the transition region (0.64) [12].

Similar to previously published simulation studies for aortic dissection [1, 10, 21], the flow was assumed to be laminar in the present study. For a pulsatile and unsteady flow, turbulence occurs at a Reynolds number that is much higher than that expected for a steady flow due to a more stable accelerating flow and a more unstable decelerating flow [1, 22]. According to Morris *et al.* [23], flow can be considered to be laminar if the maximum Reynolds number (Re_{max}) is less than the critical Reynolds number (Re_c). The critical Reynolds number (Re_c), or also called the transition Reynolds number, for unsteady flow takes the form of $Re_c=k$ x Wormersley number [24], where k ranges between 250 to 1000. As shown in Table 2, the maximum Reynolds numbers, Re_{max} for all three geometries adopted in this study were lower than their respective minimum critical Reynolds number, Re_c.

The continuity and momentum equations were used to govern blood flow in the present study, as follows:

$$\frac{\partial}{\partial t}(\rho\boldsymbol{v}) + \rho(\boldsymbol{v}.\nabla)\boldsymbol{v} = -\nabla p + \nabla.\boldsymbol{\tau} \tag{2}$$

$$\nabla.\boldsymbol{v} = 0, \tag{3}$$

The symbol $\boldsymbol{v}$ represents the velocity vector, p represents the pressure, ρ represents the density and $\boldsymbol{\tau}$ represents the stress.

2.3   Boundary Conditions

A pulsatile flow as illustrated in Figure 2 (a), with a flat velocity profile, was applied at the entrance of the ascending aorta and this is consistent with that used in previous studies [1, 25, 26]. The use of a flat velocity profile at the aortic inlet was justified based on in-vivo measurements using the hot film anemometry technique on animal models [24]. Although a recent study by Doormaal *et al.* [27] showed that the usage of a flat velocity profile could not capture the WSS at the ascending aorta accurately, they found that the effect of the inlet velocity profile in the descending aorta region, which is the focus of the present study, was negligible. Based on previous studies [1, 25], five percent of the flow volume was diverted to each branch outlet, which are left subclavian artery, left common carotid artery, and brachicephalic artery. A pulsatile pressure waveform as shown in Figure 2 (b) was applied at the exit of the descending aorta. The above-mentioned boundary conditions (at the inlet and outlet) have been used extensively in studies on diseased aorta [1, 21, 22].

2.4   Numerical Methods

The commercial CFD package of ANSYS FLUENT 14.0 (ANSYS, Inc., Canonsburg, PA, USA) was used, which is based on the finite volume method. The Second Order Upwind Scheme was used to discretize the governing equations. The PISO (Pressure Implicit with Splitting of Operators) algorithm was used for the coupling of the pressure-velocity terms. A steady state solution at the maximum flow rate during peak systole was first obtained and this solution was used as an initial condition, for unsteady pulsatile flow simulation. Five cardiac cycles were simulated for each model. After four complete cycles, cycle to cycle variations were less than 1 %. Therefore, all results presented in the current study were taken from the 5th cardiac cycle. During the post processing stage, the results were taken at four time instants (reported with reference to the beginning of the 5th cardiac cycle), i.e. at t = 0.20 s (early systole), 0.25 s (peak systole), 0.38 s (late systole) and 0.47 s (early diastole).

2.5   Mesh Independence and Time Step Sensitivity Studies

ICEM CFD, ANSYS 14.0 Inc. was used for meshing of the domain. The meshes consist of prism cells near the boundary wall and tetrahedral cells at the core region. In a simulation study investigating the mesh requirements for flow within the dissected aorta, Chen *et al.* [18] revealed that laminar simulations with near-wall mesh refinement using the prismatic boundary layer elements resulted in

similar flow patterns, including WSS and other quantities, to the k-ω SST model, with discrepancies less than 1.3% for both velocity and pressure. Thus, 15 prismatic layers were used for the near-wall mesh refinement at the boundary layer in the present study. Meanwhile, mesh dependency tests were carried out by creating three different meshes consisting of 1.92 M, 2.62 M and 3.52 M total cells, respectively, for Geometry 2. The average velocity and pressure at the entry tear region, which is both our region of interest and location with a high numerical sensitivity (due to substantial changes in the area and diversion of flow from the true lumen to the false lumen), were analyzed and shown in Table 3. The difference between the chosen mesh (2.62 M) and finer mesh (3.52 M) for both average velocity and average pressure was less than 5% and therefore, 2.62 M cell was deemed adequate for this simulation. Meanwhile, the number of elements being used was comparable with Cheng *et al.* [3], which used 2.69 M elements in their simulation for aortic dissection. The number of elements used for Geometries 1 and 3 were 2.65 M and 2.66 M, respectively.

Apart from the grid independence study, a test concerning the time step sensitivity of the unsteady simulation was also conducted. Three temporal discretization settings were tested: 0.01s (large time step), 0.005s and 0.001s. Reducing the time step from 0.005 s to 0.001 s has only resulted in a small difference in the velocity distribution (less than 5%) but significantly increased the computational cost. Thus, a time step of 0.005 s was used in the present study for computational efficiency.

2.6   Eduction Method for the Identification of Vortical Structures

For a quantitative representation of vortical structures, λ_2 method defined by Jeong and Hussain [28] was used as it is recommended to be the most suitable method for problems related to biological fluid such as blood [12]. To determine the local pressure minimum due to vortical motion, the eigenvalues of the $S^2 + \Omega^2$ tensor (the symmetric (S) and antisymmetric (Ω) parts of the velocity gradient tensor) were calculated [29]. Ranking the eigenvalues as $\lambda_1 > \lambda_2 > \lambda_3$, the presence of vortical structures was defined as regions with negative λ_2 [12]. For the purpose of providing a clearer illustration, a threshold value, $\lambda_{2,t}$ equivalent to -12.5s^{-2} was applied to reduce the number of vortical regions [12, 30]. The λ_2 intensity in the whole blood domain was calculated using the following equation:

$$\int \omega dV_{fluid} \tag{4}$$

where dV_{fluid} is the fluid domain and ω is the vorticity.

In the present study, we analyzed vortical structures by distinguishing spanwise vortices from streamwise vortices, as proposed by Biasetti et al. [12]. Vortical structures originate from the shear layer near the wall where a region of high velocity gradient exists [12]. Spanwise vortical structures were formed when this unstable shear layer undergoes a Kelvin-Helmholtz instability, leading to a rolled up layer of vorticity [12]. In contrary, unstable low speed streaks trigger the formation of streamwise vortical structures, where sheets of streamwise vorticity collapse into streamwise vortices by a stretching rather than a roll up mechanism [12]. The nonlinear process of pairing, tearing and reconnection in vortical structures causes them to move, develop and interact among each other [12].

2.7   Prediction of the Location for Thrombus Extension

The breakdown of vortical structures into streamwise substructures released the platelets which would subsequently adhere to low WSS location, leading to the formation of thrombus. Therefore, in order to predict the location of thrombus extension, we superimposed WSS contour on the vortical structures distribution. The location of thrombus extension can be predicted at the regions where vortical structures show break up (due to a lost in strength) with low velocity and WSS (< 0.5 Pa) [14-16].

3.0 RESULTS

3.1 Flow patterns and pressure distribution

Figure 3 shows the velocity streamline superimposed on the vortical structures in the original geometry at peak systole, using the Newtonian model. Consistent with previously published in vitro experimental [31] and CFD simulation studies [3, 9, 21, 32] on aortic dissection, strong jet-like flow passed through the entry tear region and impinged onto the posterior region of the false lumen wall. Recirculation zones with dominant vortical structures were observed around the entry tear, as previously shown in both initial and follow up studies using phase-contrast magnetic resonance images (PC-MRI) [9] as well as in vitro experimental studies [31]. Consequently, high shear gradient was generated, resulting in high, localized WSS at this region. Both our peak systolic velocity (170 cm/s) and maximum time average wall shear stress (TAWSS) (6.73 Pa) coincides with previously published values (i.e. up to 180 cm/s [4] for large tears and 6.92 – 14.1 Pa at the throat of the coarctation [1].

With regards to the pressure distribution, the pressure in the true lumen was generally higher than that in the false lumen in the proximal portion but opposite in the distal portion at peak systole (Figure 4), as observed in both in vitro experimental [33] and simulation [1, 3] studies. To the contrary, proximal false lumen pressure was slightly higher as compared to true lumen during diastole.

3.2 Evolution of vortical structures in the false lumen region throughout a cardiac cycle

The region of interest in this study was the false lumen region. Region labeled with A was located above the entry tear region while regions labeled with B, C and D were located at the entry tear and below the entry tear region. As shown in Figure 5, aggregated vortical structures were found above the entry tear region during early systole (zoom in Label A1) while these vortical structures were found to be slightly reduced in size during peak systole (zoom in Label A2). Below this, i.e. around the entry tear region, vortical structures observed during early systole (Label B1) were found to develop into a ring-shaped pattern during peak systole (Label B2). Meanwhile, below the entry tear region, vortical structures which exists (Label C1) during early systole were observed to move slightly downstream during peak systole (Label C2). At the distal part of the false lumen, more distinct

spanwise vortical structures could be observed during peak systole (Label D1) as compared to early systole, especially at the inner part of the curvature. The interaction between the vortical structures with the boundary layer caused a localized region of high WSS at the coarctation (12.43 Pa during peak systole) and the entry tear region (14.70 Pa during peak systole) (Figure 6).

As compared to peak systole, the ring-shaped vortical structures found around the entry tear entrance region (Label B2) expanded and accumulated around and below the region (from approximately 20 mm to 80 mm) during late systole and early diastole (Labels B3 and B4) respectively. Meanwhile, vortical structures that were located downstream of the entry tear (Label C2) during peak systole were found to have broken down into several streamwise substructures during late systole and early diastole (Label C3 and Label C4). Less spanwise vortical structures were found at the distal part of the false lumen during late systole (Label D2) and early diastole (Label D3).

Figure 7 shows the superimposition of the WSS contour and the vortical structures distribution during early diastole. Based on our analysis (Figures 5, 6 and 7) following the method described in Section 2.7, we predict that thrombus would form at the posterior region of the false lumen wall, extending up to 56 mm below the entry tear (Label C4 in Figure 5, corresponding to the circular region in Figure 7).

3.3   Effect of non-Newtonian (Carreau-Yasuda) property on vortical structures and WSS

As compared to the Newtonian model, though the distribution of the spanwise vortical structures for the Carreau-Yasuda model showed no significant difference, a lower number of streamwise vortical structures with smaller sizes were observed in the Carreau-Yasuda model (results not shown). In terms of quantitative representation based on λ_2 intensity in the blood vessel domain (Table 4), some significant differences were seen between these two models at early systole, peak systole and early diastole. For example, the Newtonian model predicted up to 8.12% more vortical structures per volume of fluid at early systole as compared to the Carreau-Yasuda model. Among the four cardiac phases, minimum percentage difference in λ_2 intensity was found during late systole, with the Newtonian model having slightly higher λ_2 intensity (2.44%) as compared to the Carreau-Yasuda model.

3.4   Effect of false lumen size on vortical structures and WSS using Carreau-Yasuda model

Since Carreau-Yasuda model is expected to present blood rheology more accurately, it was used in this section. Among the three geometries used in the present study, Geometry 2 has the largest false lumen diameter, followed by Geometry 1 and 3. From our analysis, the changes or trend of the vortical structures and WSS results in our simulation study are very much dependent on the changes in the false lumen sizes.

As demonstrated in Table 5, a significant difference with regards to the quantitative representation based on the λ_2 intensity can be seen among the different geometries with varying false lumen sizes, especially during early and peak systole. Higher λ_2 intensity was achieved with an increase in the false lumen size in all cardiac phases. In particular, Geometry 2 with the largest false lumen diameter predicted up to 51.58 % more vortical structures per volume of fluid at early systole as compared to Geometry 1 with a smaller false lumen diameter. Among the four cardiac phases, minimum percentage difference in λ_2 intensity was found during late systole and early diastole. Meanwhile, our simulation results (Figure 8) showed that the percentage of flow entering the false lumen increased with an increase in the false lumen size. On the other hand, the predicted location of thrombus

formation (based on our analysis method described in Section 3.2) appeared to be extended further away from the entry tear region with increasing false lumen size.

The distributions of WSS were similar in both geometries despite a difference in their relative magnitudes (not shown). During early systole and peak systole, high WSS was observed at the coarctation region at the exit of the aortic arch and at the entry tear region, coincident with regions accumulated with spanwise vortical structures. Regions of low WSS was observed at the distal region of the posterior false lumen wall. Geometry 2 with the largest false lumen diameter demonstrated the highest maximum WSS value during peak systole at the entry tear region (21.04 Pa vs. 15.01 Pa for Geometry 3 with the smallest false lumen diameter), but the lowest minimum WSS value (0.42 Pa vs. 0.58 Pa for Geometry 3 at the posterior false lumen region, accounting for a difference of 32.9%).

4.0   DISCUSSION

To the best of our knowledge, this is the first study attempting to explain and predict the location of thrombus in an aortic dissection case with complicated geometrical feature both qualitatively and quantitatively, based on the evolution of vortical structures and their interaction with the WSS in the false lumen region throughout a cardiac cycle. In the present study, vortical structures were seen to occupy the entire false lumen region (except at a few locations) over the whole cardiac cycle (Figures 5). The presence of recirculation zones with dominant vortical structures, together with the action of the high WSS surrounding the entry tear, is believed to cause platelet activation [12]. The strong jet-like flow through the entry tear pushed the reattachment point downstream, and contributed to the growth of the vortical structures [14]. The growth and accumulation of the vortical structures around and below the entry tear region continued throughout peak and late systole (reflected by an increase in λ_2 intensity, Tables 4 & 5), causing repeated collision of platelets for a long period of time [35], and is believed to result in the spontaneous formation of the platelet aggregates [12]. During late systole and early diastole, the flow had lost its strength and as a result the vortical structures were seen to have broken down into several streamwise substructures. The breakup of vortical structures released the platelets which were subsequently adhered to the low WSS location at the posterior region of the false lumen wall, leading to the formation of thrombus.

Based on the above analysis, we predict a tendency of the formation and thickening of thrombus at the posterior false lumen wall in our geometry, distal to the entry tear region, over a finite period of time. To date, two separate longitudinal studies [4, 9] have been carried out to predict the location of thrombus formation, with one study performed on a chronic dissection patient [9] and another using sequential follow up scans on a patient with acute dissection [4]. In Karmonik *et al.*'s [9] study on a chronic dissection patient, a hypointense region was observed in the MRI images after contrast injection at the posterior thoracic false lumen wall during both initial examination and at a 10-month follow-up examination when significant aneurismal dilatation occurred, which they believed to represent thrombus formation. Cheng *et al.* [4] performed seven consecutive scans over a year on an acute dissection patient with no significant aneurismal dilatation, and they reported the formation of

thrombus at the posterior false lumen region below the entry tear, which extended downward along the wall during follow-up examinations. Similar to both studies, the posterior false lumen wall in our geometry was located opposite to the line of intimal flap. As reported in previous studies [6, 8], formation of a partial thrombus in the false lumen region may occlude distal reentry tears, leading to high diastolic pressure, increased wall tension and elevated risk of aneurismal dilatation or rupture, particularly at the proximal false lumen site. Furthermore, intraluminal thrombosis has been reported to cause local inflammation and localized wall weakening [7], in particular in the false lumen region which already had reduced wall strength. In addition, high WSS observed at the coarctation throat may cause additional injury to the endothelial cells, leading to an expansion of the entry tear [1].

Although false lumen size has been recognized as an important risk factor for rapid aneurismal growth [5] and increased chance of thrombosis [6], the mechanism behind this remains to be clarified. In the present study, we investigated the effect of false lumen size on the risk of thrombus formation using vortical structures presentation by modifying the original patient specific geometry. Our simulation results demonstrated a more dominant vortical structures and higher λ_2 intensity with increasing false lumen size. In addition, consistent with previously published findings [1, 3], higher maximum WSS value was encountered at the bended throat of coarctation, with an increase in the percentage of flow entering the false lumen. Based on the interrelationship among vortical structures, WSS and thrombus formation described before, our observations could explain the increased chance of thrombus formation in patients with false lumen dilatation [12]. Apart from that, our analysis results showed that the predicted location of thrombus formation appeared to be extended further away from the entry tear region with increasing false lumen size. We believed that this is caused by an associated increase in the false lumen flow rate and λ_2 intensity, which pushed the vortical structures further downstream. Our findings were consistent with a longitudinal study [4], which demonstrated a downward shift of the areas of thrombus formation during sequential follow up scans in a patient with acute dissection, which showed a significant increase in the primary tear size and false lumen flow rate. Formation of thrombus further away from the entry tear region could increase the chance of dissected aorta with the

sac-formation type (i.e. that involves coverage of the distal reentry tear), which has been shown to cause a substantial increase in the growth rate of the false lumen [6].

A non-Newtonian model is known to be able to capture blood rheology more accurately as compared to a Newtonian model [12]. To date, only Cheng *et al*. [3] have looked at the effect of rheological properties in aortic dissection cases using the Quemada model. Their results revealed that the inclusion of a non-Newtonian model caused a reduction in the maximum WSS value (~8%) and either an extension or reduction in the turbulence intensity at different regions along the vessel. Both graphical and quantitative presentation of vortical structures in our simulation results revealed that the Newtonian model overestimated streamwise vortical structures in the false lumen. This is in agreement with Biasetti *et al*. [12] findings, which suggested that streamwise vortical structures might be an artifact of the Newtonian model. The shear thinning behavior of the Non-Newtonian model was able to capture the increase in viscosity in the core flow region, thus suppressing the development of streamwise vortical structures [12].

As this is a preliminary study to describe the evolution of vortical structures and their interaction with the WSS in aortic dissection cases, CT images of only one patient during initial examination were used, and no follow up studies were performed to confirm our predicted location of thrombus formation. In spite of this, the process by which vortices and shear stress influence platelet activity (i.e. activation, aggregation and deposition), which served as the basis of this study, has been well established numerically and validated experimentally in previous publications [14-16]. Furthermore, as shown in Section 3.1, with regards to hemodynamic variables, our simulation results were comparable with previously published clinical and experimental findings. Future studies involving more patients with different aortic dissection configurations, obtained at both initial examination and during follow up studies, will be carried out to ascertain the predictive value of the vortical structures on thrombus formation.

5.0   LIMITATIONS

There are several limitations associated with the present study. The aortic wall was assumed to be rigid. This is justified to be a reasonable assumption given the fact that the compliance of an aneurysmal blood vessel is significantly reduced due to the lack of elastin [36]. As described in Section 2.2, in vivo data have shown a significant reduction in the vessel wall distensibility in type B aortic dissection patients, and consequently no appreciable vessel wall movement was observed in the cine MRI images over a cardiac cycle [19]. Furthermore, the main difficulty in assuming the wall of aorta and aortic dissection to be elastic is that the vessel wall contains both healthy and diseased tissue, for which the exact material properties are difficult to be ascertained.

In the present study, laminar flow model was adopted based on our calculation results which showed that the maximum Reynolds numbers for all three geometries were lower than their respective ranges for critical Reynolds number. Furthermore, near wall mesh refinement using 15 prismatic boundary layer elements was adopted in the present study, based on simulation findings by Chen *et al.* [18] who revealed that a minimum of 10 prismatic layers for the boundary layer was fine enough to yield similar flow patterns as the k-ω SST model. While the present study focuses on qualitative presentation of vortical structures, on-going studies using transitional SST model are being carried out in our laboratory, focusing on quantitative assessment of the vortical structure parameters.

6.0   CONCLUSION

In conclusion, this study shows that:

- The evolution of vortical structures throughout a cardiac cycle and their interaction with the WSS provided insight to the potential mechanism behind the development and progression of thrombus in the false lumen region.

- Higher λ_2 intensity, associated with higher maximum WSS and lower minimum WSS, was achieved with an increase in the false lumen size, and we believed that this increases the risk of thrombus formation and thus aneurismal dilatation.

- The percentage of the flow entering the false lumen increased with an increase in the false lumen size, leading to a downward shift of the areas of thrombus formation along the false lumen wall.

CONFLICT OF INTEREST

There is no conflict of interest in this work

REFERENCES:

[1] K.M. Tse, P. Chiu, H.P. Lee, P. Ho, Investigation of hemodynamics in the development of dissecting aneurysm within patient-specific dissecting aneurismal aortas using computational fluid dynamics (CFD) simulations, Journal of Biomechanics, 44 (2011) 827-836.

[2] S.G. Thrumurthy, A. Karthikesalingam, B.O. Patterson, P.J.E. Holt, M.M. Thompson, The diagnosis and management of aortic dissection, British Medical Journal, 344 (2012) 37-42.

[3] Z. Cheng, F.P.P. Tan, C.V. Riga, C.D. Bicknell, M.S. Hamady, R.G.J. Gibbs, N.B. Wood, X.Y. Xu, Analysis of flow patterns in a patient-specific aortic dissection model, Journal of Biomechanical Engineering, 132 (2010) 051007-051001-051007-051009.

[4] Z. Cheng, C. Riga, J. Chan, M. Hamady, N.B. Wood, N.J.W. Cheshire, Y. Xu, R.G.J. Gibbs, Initial findings and potential applicability of computational simulation of the aorta in acute type B dissection, Journal of Vascular Surgery, 57 (2013) 35S-43S.

[5] A. Marui, T. Mochizuki, M. Norimasa, T. Koyama, F. Kimura, M. Horibe, Toward the best treatment for uncomplicated patients with Type B acute aortic dissection : A consideration for sound surgical indication, Circulation, 100 (1999) II-275-II-280.

[6] S. Trimarchi, J.L. Tolenaar, F.H. Jonker, B. Murray, T.T. Tsai, K.A. Eagle, V. Rampoldi, H.J. Verhagen, J.A. van Herwaarden, F.L. Moll, Importance of false lumen thrombosis in type B aortic dissection prognosis, The Journal of Thoracic and Cardiovascular Surgery, 145 (2013) S208-S212.

[7] E. Sueyoshi, I. Sakamoto, M. Uetani, Growth rate of affected aorta in patients with type B partially closed aortic dissection, The Annals of Thoracic Surgery, 88 (2009) 1251-1257.

[8] T.T. Tsai, A. Evangelista, C.A. Nienaber, T. Myrmel, G. Meinhardt, J.V. Cooper, D.E. Smith, T. Suzuki, R. Fattori, A. Llovet, Partial thrombosis of the false lumen in patients with acute type B aortic dissection, New England Journal of Medicine, 357 (2007) 349-359.

[9] C. Karmonik, S. Partovi, M. Muller-Eschner, J. Bismuth, M.G. Davies, D.J. Shah, M. Loebe, D. Bockler, A.B. Lumsden, H. von Tengg-Kobligk, Longitudinal computational fluid dynamics study of aneurysmal dilation in a chronic DeBakey type III aortic dissection, Journal of Vascular Surgery, 56 (2012) 260-263.

[10] W.N. Wan Ab Naim, P. Ganesan, Z. Sun, K. Osman, E. Lim, The impact of the number of tears in patient-specific Standford type B aortic dissecting aneurysm: CFD simulation, Journal of Mechanics in Medicine and Biology, 13 (2014) 1450017-1450011-1450020.

[11] Y. Fan, S.W.K. Cheng, K.X. Qing, K.W. Chow, Endovascular repair of type B aortic dissection : a study by computational fluid dynamics, Journal of Biomedical Science and Engineering, 3 (2010) 900-907.

[12] J. Biasetti, F. Hussain, C. Gasser, Blood flow and coherent vortices in the normal and aneurysmatic aortas: a fluid dynamical approach to intra-luminal thrombus formation, Journal of the Royal Society Interface, 8 (2011) 1449-1461.

[13] J. Biasetti, Physics of blood flow in arteries and its relation to intra-luminal thrombus and atherosclerosis, in: KTH School of Engineering Sciences, Department of Solid Mechanics - vascuMECH, KTH Royal Institute of Technology, Sweden, 2013, pp. 43.

[14] S. Einav, D. Bluestein, Dynamics of blood flow and platelet transport in pathological vessels, Annals New York Academy of Sciences, 1015 (2004) 351-366.

[15] D. Bluestein, C. Gutierrez, M. Londono, R.T. Schoephoerster, Vortex shedding in steady flow through a model of an arterial stenosis and its relevance to mural platelet deposition, Annals of Biomedical Engineering, 27 (1999) 763-773.

[16] S. Raz, S. Einav, Y. Alemu, D. Bluestein, DPIV prediction of flow induced platelet activation-Comparison to numerical predictions, Annals of Biomedical Engineering, 35 (2007) 493-504.

[17] C.P. Chang, J.C. Liu, Y.M. Liou, S.S. Chang, J.Y. Chen, The role of false lumen size in prediction of in-hospital complications after acute type B aortic dissection, Journal of the American College of Cardiology, 52 (2008) 1170-1176.

[18] D. Chen, M. Muller-Eschner, H. von Tengg-Kobligk, D. Barber, D. Bockler, R. Hose, Y. Ventikos, A patient-specific study of type-B aortic dissection: evaluation of true-false lumen blood exchange, BioMedical Engineering Online, 12 (2013) 1-16.

[19] M.K. Ganten, T.F. Weber, H. von Tengg-Kobligk, D. Böckler, W. Stiller, P. Geisbüsch, G.W. Kauffmann, S. Delorme, M. Bock, H.-U. Kauczor, Motion characterization of aortic wall and intimal flap by ECG-gated CT in patients with chronic B-dissection, European Journal of Radiology, 72 (2009) 146-153.

[20] F.J.H. Gijsen, F.N. van de Vosse, J.D. Janssen, The influence of the non-Newtonian properties of blood on the flow in large arteries: steady flow in a carotid bifurcation model, Journal of Biomechanics, 32 (1999) 601-608.

[21] D. Chen, M. Muller-Eschner, D. Kotelis, D. Bockler, Y. Ventikos, H. Von Tengg-Kobligk, A longitudinal study of Type-B aortic dissection and endovascular repair scenarios: Computational analyses, Medical Engineering and Physics, 35 (2013) 1321-1330.

[22] S.K. Lam, G.S.K. Fung, S.W.K. Cheng, K.W. Chow, A computational study on the biomechanical factors related to stent-graft models in the thoracic aorta, Medical and Biological Engineering and Computing, 46 (2008) 1129-1138.

[23] L. Morris, P. Delassus, A. Callanan, M. Walsh, F. Wallis, P. Grace, T. McGloughlin, 3-D Numerical Simulation of blood flow through models of the human aorta., Journal of Biomechanical Engineering, 127 (2005) 767-775.

[24] R. Nerem, W.A. Seed, N.B. Wood, An experimental study of the velocity distribution and transition to turbulence in the aorta, Journal of Fluid Mechanics, 52 (1972) 137-160.

[25] M.S. Olufsen, C.S. Peskin, W.Y. Kim, E.M. Pedersen, A. Nadim, J. Larsen, Numerical simulation and experimental validation of blood flow in arteries with structured-tree outflow conditions, Annals of Biomedical Engineering, 28 (2000) 1281-1299.

[26] C.Y. Wen, A.S. Yang, L.Y. Tseng, J.W. Chai, Investigation of pulsatile flowfield in healthy thoracic aorta models, Annals of Biomedical Engineering, 38 (2010) 391-402.

[27] M.A. Van Doormaal, A. Kazakidi, M. Wylezinska, A. Hunt, J.L. Tremoleda, A. Protti, Y. Bohraus, W. Gsell, P.D. Weinberg, C.R. Ethier, Haemodynamics in the mouse aortic arch computed from MRI-derived velocities at the aortic root, Journal of The Royal Society Interface, (2012) 1-11.

[28] J. Jeong, F. Hussain, On the identification of a vortex, Journal of Fluid Mechanics, 285 (1995) 69-94.

[29] O. Pierakos, P.P. Vlachos, The effect of vortex formation on left ventricular filling and mitral valve efficiency, Journal of Biomechanical Engineering, 128 (2006) 527-539.

[30] S. Loerakker, L.G.E. Cox, G.J.F. van Heijst, B.A.J.M. de Mol, F.N. van de Vosse, Influence of dilated cardiomyopathy and a left ventricular assist device on vortex dynamics in the left ventricle, Computer Methods in Biomechanics and Biomechanical Engineering, 11 (2008) 649-660.

[31] P.A. Rudenick, B.H. Bijnens, D. García-Dorado, A. Evangelista, An in vitro phantom study on the influence of tear size and configuration on the hemodynamics of the lumina in chronic type B aortic dissections, Journal of Vascular Surgery, 57 (2013) 464-474.

[32] A. Rinaudo, G. D'Ancona, J.J. Lee, G. Pilato, A. Amaducci, R. Baglini, F. Follis, M. Pilato, S. Pasta, Predicting outcome of aortic sissection with patent false lumen by computational flow analysis, Cardiovascular Engineering and Technology, 5 (2014) 176-188.

[33] T.T. Tsai, M.S. Schlicht, K. Khanafer, J.L. Bull, D.T. Valassis, D.M. Williams, R. Berguer, K.A. Eagle, Tear size and location impacts false lumen pressure in an ex vivo model of chronic type B aortic dissection, Journal of Vascular Surgery, 47 (2008) 844-851.

[34] P. Chakraborty, S. Balachandar, R.J. Adrian, On the relationships between local vortex identification schemes, Journal of Fluid Mechanics, 535 (2005) 189-214.

[35] F.J. Tovar-Lopez, G. Rosengarten, M. Nasabi, V. Sivan, K. Khosmanesh, S.P. Jackson, A. Mitchell, W.S. Nesbitt, An investigation on platelet trasnport during thrombus formation at micro-scale stenosis, PLOS One, 8 (2013) e74123-e74134.

[36] L. Boussel, V. Rayz, A. Martin, G. Acevedo-Bolton, M.T. Lawton, R. Higashida, W.S. Smith, W.L. Young, D. Saloner, Phase-contrast magnetic resonance imaging measurements in intracranial aneurysms in vivo of flow patterns, velocity fields, and wall shear stress: Comparison with computational fluid dynamics, Magnetic Resonance in Medicine, 61 (2009) 409-417.

TABLES:

Geometry	Plane	Diameter (mm)	
		Aorta	False lumen
Geometry 1	A	37.9	25.2
	B	56.0	24.8
	C	41.8	26.0
Geometry 2	A	40.2	27.5
	B	57.1	26.8
	C	44.0	28.1
Geometry 3	A	34.8	22.1
	B	53.5	22.1
	C	39.0	23.0

Table 1: The dimensions of the aorta and the false lumen at three different planes for the original (Geometry 1) and modified geometries (Geometries 2 and 3).

	Geometry 1	Geometry 2	Geometry 3
Maximum Reynolds number, Re_{max}	4570	3826	4533
Average Wormersley number	20.8	21.3	20.0
Minimum Critical Reynolds number, Re_c	5193	5325	5016

Table 2: The maximum and critical Reynolds number, as well as Wormersley number for Geometries 1, 2 and 3.

Number of cells	Average velocity (m./s)	Differences (%)	Average pressure (Pa)	Differences (%)
1 915 996	0.26		1105.65	
2 628 175	0.23	12.3	1093.95	1.1
3 521 903	0.24	3.9	1147.12	4.7

Table 3: Results of mesh independent test of comparison of average velocity and maximum pressure between meshes

Cardiac phase	New	C-Y	Diff New-CY (%)
Early systole	-0.0084	-0.0078	8.12
Peak systole	-0.0192	-0.0180	6.67
Late systole	-0.0303	-0.0311	2.44
Early diastole	-0.0235	-0.0222	5.89

Table 4: Comparison of the λ_2 intensity (m^3/s^2) in the whole blood domain between the Newtonian (New) model and the Carreau-Yasuda (C-Y) model

Cardiac phase	G1	G2	G3	Diff G1-G2 (%)	Diff G1- G3 (%)
Early systole	-0.0078	-0.0128	-0.0069	51.58	12.29
Peak systole	-0.018	-0.0223	-0.0142	21.59	23.94
Late systole	-0.0311	-0.031	-0.026	0.32	18.01
Early diastole	-0.0222	-0.0216	-0.0208	2.74	6.52

Table 5: Comparison of the λ_2 intensity (m^3/s^2) in the whole blood domain for Carreau-Yasuda model for Geometry 1 (G1), Geometry 2 (G2) and Geometry 3 (G3)

FIGURES:
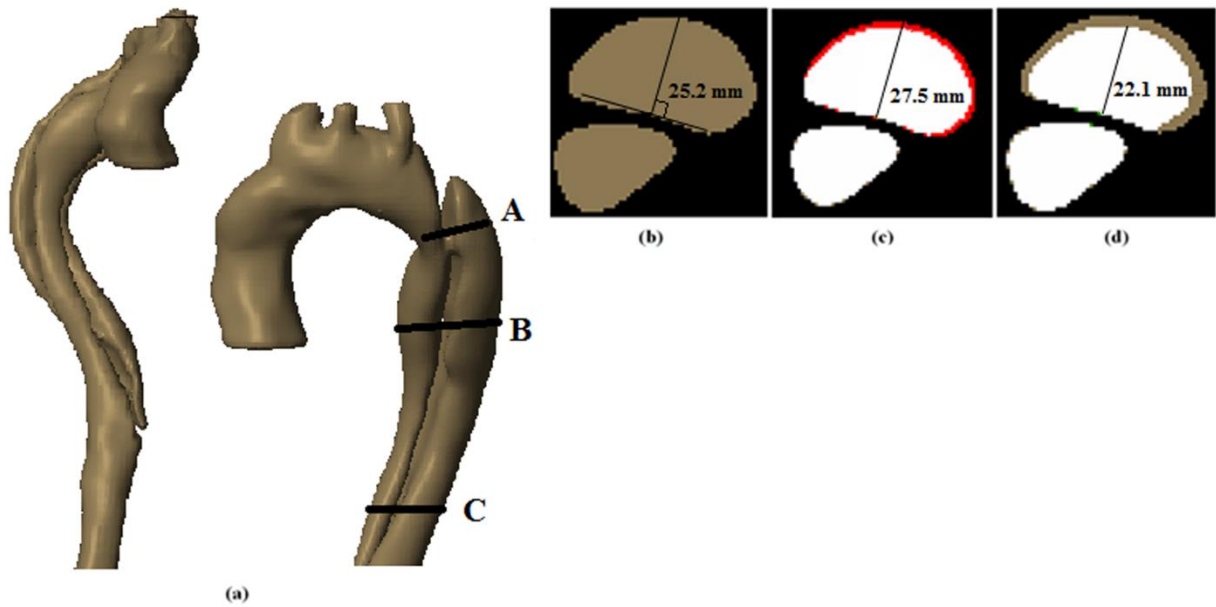
Figure 1: (a) 3D reconstructed model of the aortic dissection with labeling of Plane A, Plane B and Plane C; (b) cross sectional image of Geometry 1 at Plane A; (c) cross sectional image of Geometry 2 (red) overlapped with Geometry 1 (white) at Plane A; and (d) cross sectional image of Geometry 3 (white) overlapped with Geometry 1 (brown) at Plane A.
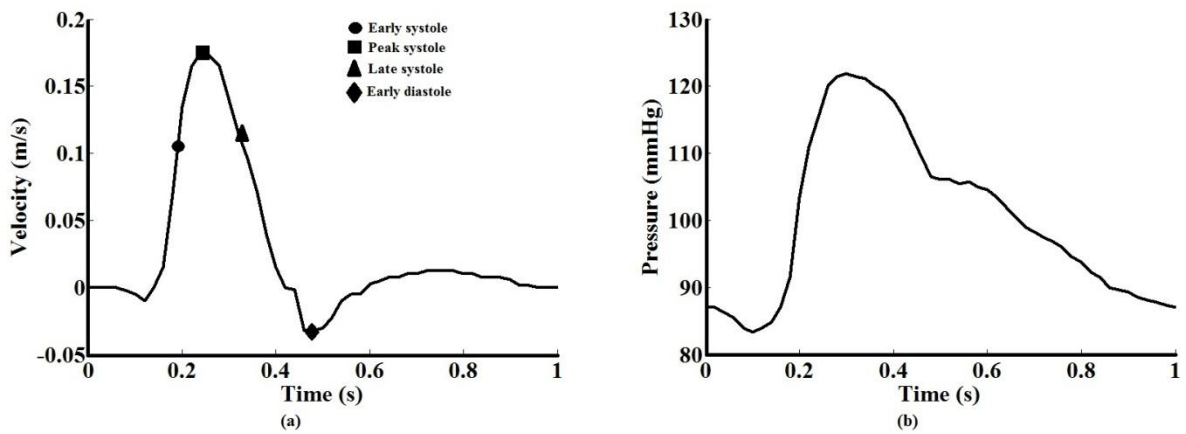
Figure 2: Inlet and outlet boundary conditions: (a) pulsatile inlet velocity profile; (b) pulsatile outlet pressure profile. Adapted from references [1, 25]
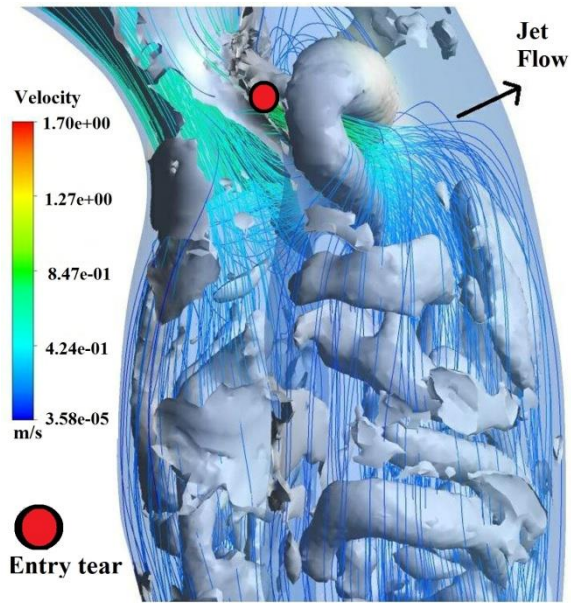
Figure 3: Jet flow passing through the entry tear where recirculation zones with dominant vortical structures were observed around the entry tear as well as at the false lumen region.
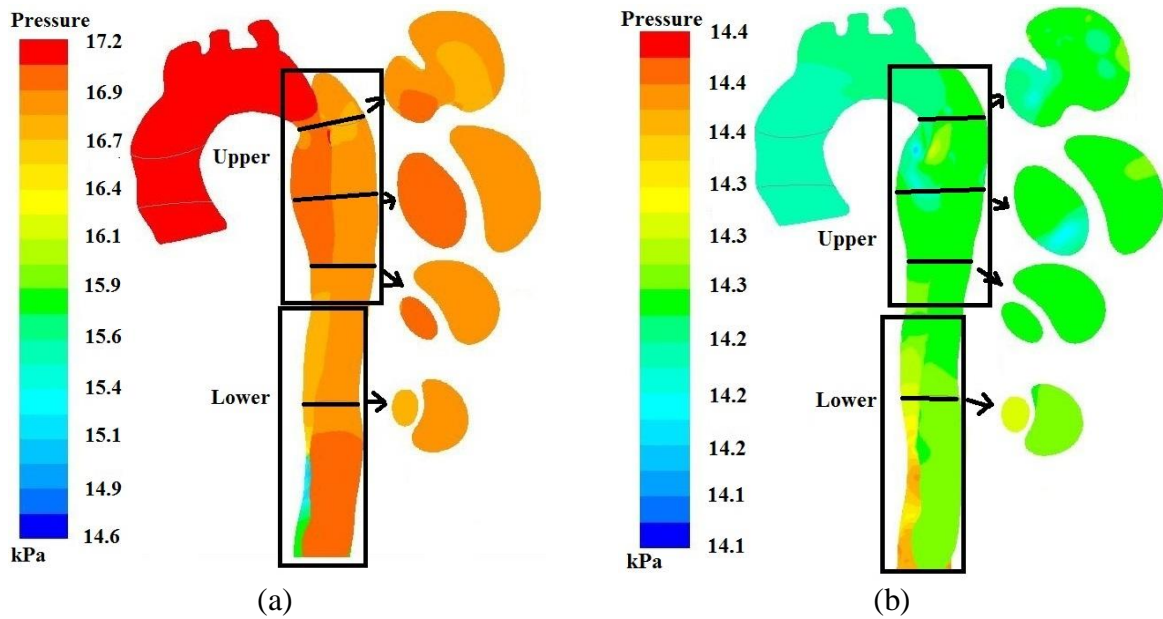
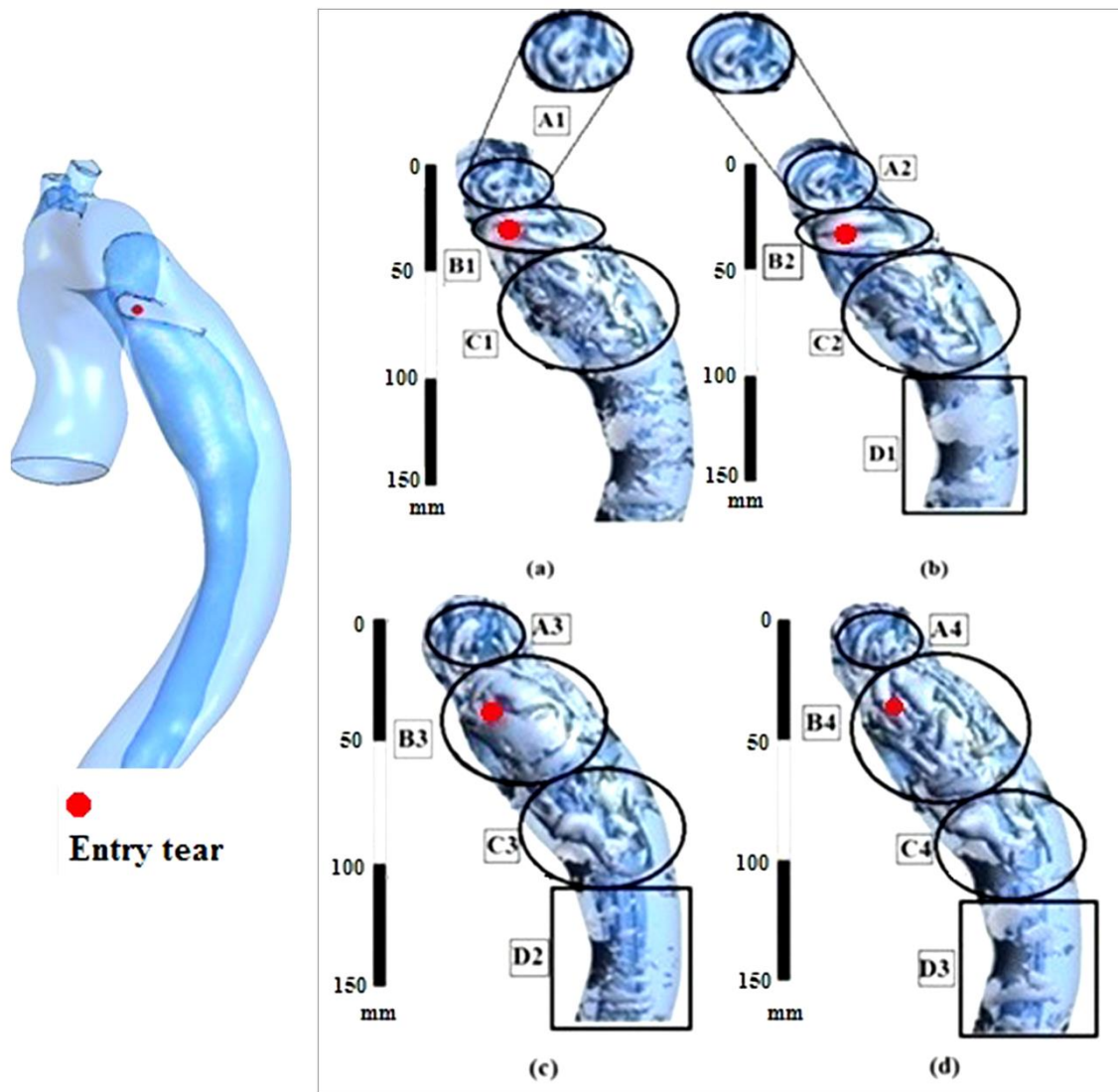Figure 4: Pressure distribution in the true and false lumen regions at (a) peak systole and (b) early diastole.

Figure 5: Vortical structures ($\lambda_{2,t}$ equal to -12.5 s^{-2}) distribution for Newtonian model at (a) early systole; (b) peak systole; (c) late systole and (d) early diastole.
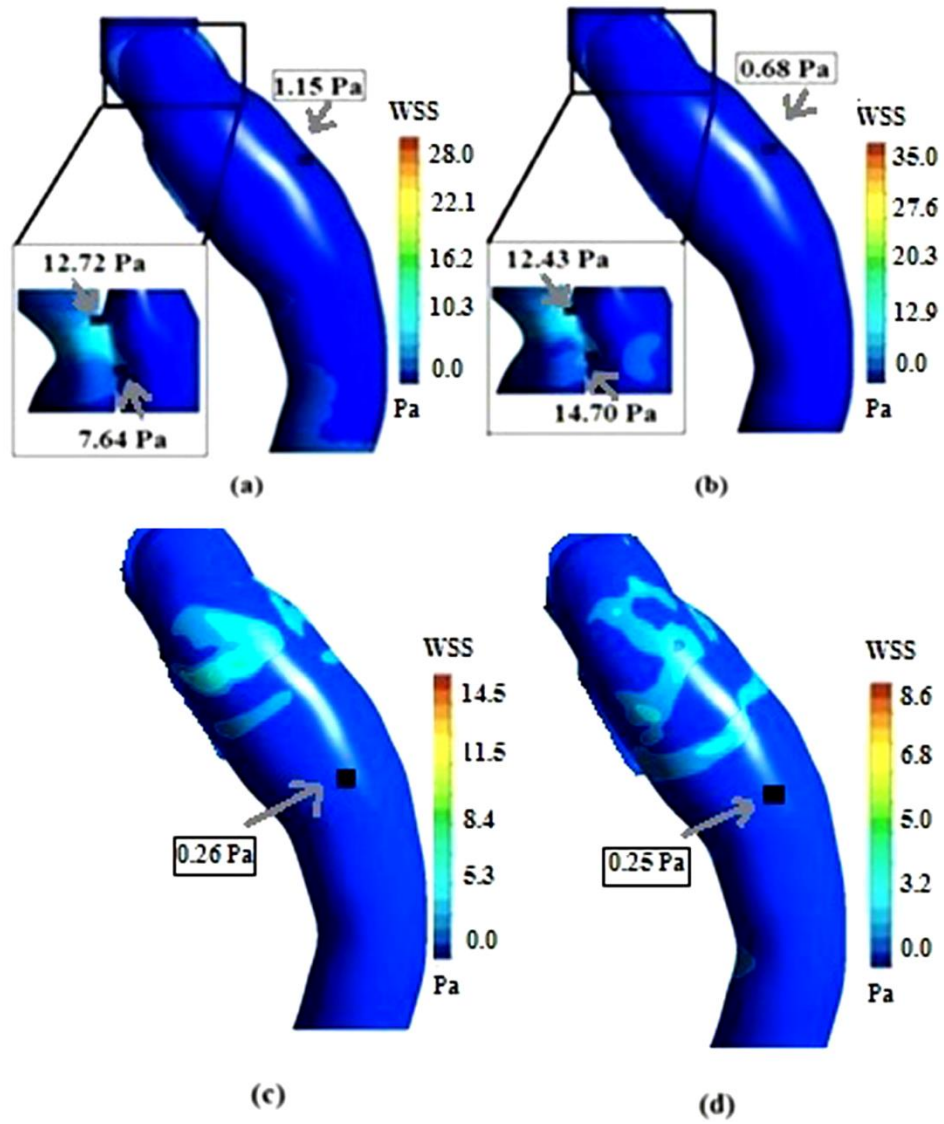
Figure 6: Contour of WSS distribution for Newtonian model at (a) early systole; (b) peak systole; (c) late systole and (d) early diastole.
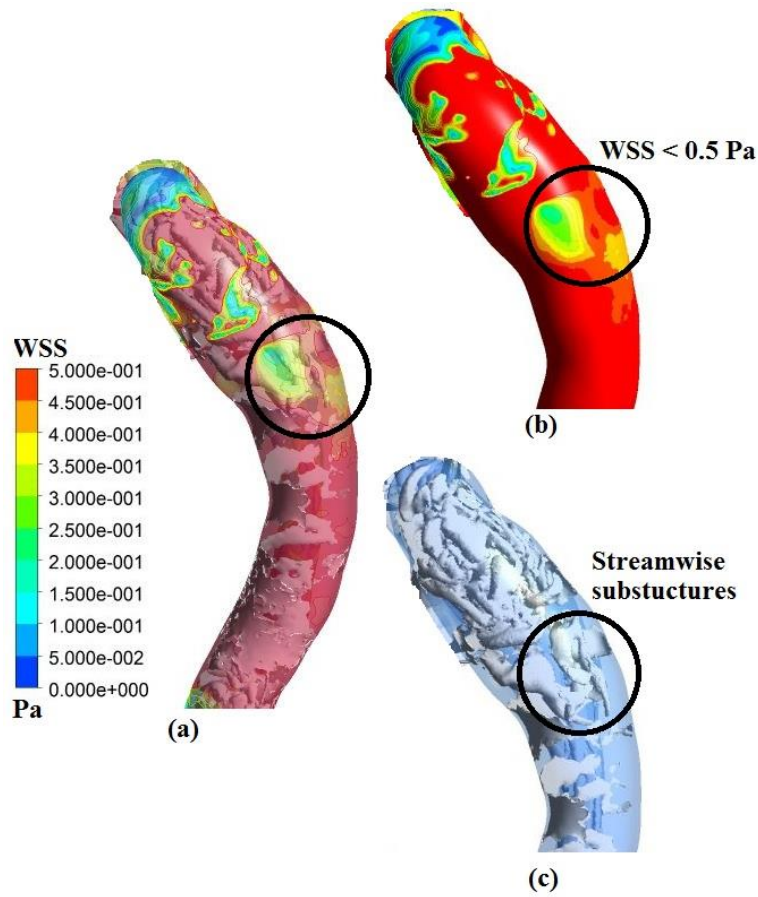
Figure 7: (a) WSS contour superimposed on vortical structures; (b) Contour of WSS (range between 0 to 0.5 Pa) and (c) Vortical structures distribution ($\lambda_{2,t}$ equal to -12.5 s^{-2}) during early diastole.
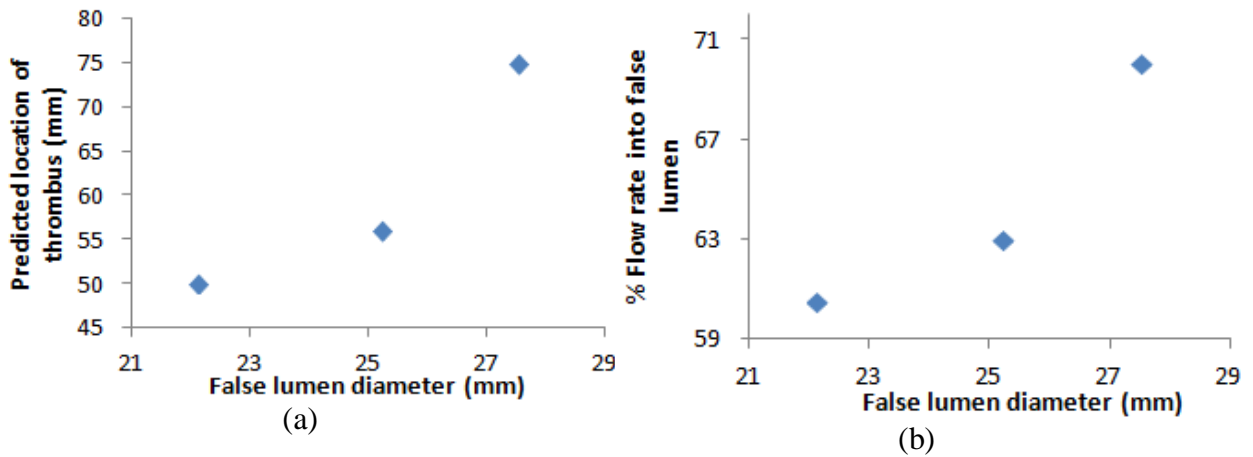

Fig 8: (a) Predicted location of thrombus extension (measured from the entry tear location) and (b) percentage of flow entering the false lumen for 3 different geometries with varying false lumen diameters (measured at plane A as shown in Figure 1).